

Article

# Relating Sentinel-1 Interferometric Coherence to Mowing Events on Grasslands

Tanel Tamm <sup>1,2,\*</sup>, Karlis Zalite <sup>2,3,4</sup>, Kaupo Voormansik <sup>2,3</sup> and Liina Talgre <sup>5</sup>

<sup>1</sup> Department of Geography, University of Tartu, Vanemuise 46, 51014 Tartu, Estonia

<sup>2</sup> KappaZeta Ltd., Mäeallika, 71508 Suure-Jaani, Estonia; karlis.zalite@to.ee (K.Z.);  
kaupo.voormansik@to.ee (K.V.)

<sup>3</sup> Department of Remote Sensing, Tartu Observatory, 61602 Tõravere, Estonia

<sup>4</sup> Department of Physical Geography and Ecosystem Science, Lund University, Sölvegatan 12,  
S-223 62 Lund, Sweden

<sup>5</sup> Department of Field Crop and Grassland Husbandry, Estonian University of Life Sciences, Kreutzwaldi 1,  
51014 Tartu, Estonia; liina.talgre@emu.ee

\* Correspondence: tanel.tamm@ut.ee; Tel.: +372-737-5086

Academic Editors: James Campbell and Prasad S. Thenkabail

Received: 1 July 2016; Accepted: 15 September 2016; Published: 27 September 2016

**Abstract:** In this study, the interferometric coherence calculated from 12-day Sentinel-1 image pairs was analysed in relation to mowing events on agricultural grasslands. Results showed that after a mowing event, median VH (vertical transmit, horizontal receive) and VV (vertical transmit, vertical receive) polarisation coherence values were statistically significantly higher than those from before the event. The shorter the time interval after the mowing event and the first interferometric acquisition, the higher the coherence. The coherence tended to stay higher, even 24 to 36 days after a mowing event. Precipitation caused the coherence to decrease, impeding the detection of a mowing event. Given the three analysed acquisition geometries, it was concluded that afternoon acquisitions and steeper incidence angles were more useful in the context of this study. In the case of morning acquisitions, dew might have caused a decrease of coherence for mowed and unmowed grasslands. Additionally, an increase of coherence after a mowing event was not evident during the rapid growth phase, due to the 12-day separation between the interferometric acquisitions. In future studies, six-day pairs utilising Sentinel-1A and 1B acquisitions should be considered.

**Keywords:** synthetic aperture radar; SAR, mowing detection; grasslands; agriculture; interferometric coherence; weather radar; precipitation estimates

## 1. Introduction

Almost all life on Earth depends inevitably on primary production. Grasslands are efficient producers of organic matter, having a high net primary production (NPP) to gross primary production (GPP) ratio, NPP/GPP. Zhao et al. [1] reported that for grasslands, the three-year mean NPP/GPP ratio estimated with the improved MODIS 1 km × 1 km grid MOD17 product is 0.65, while for deciduous broadleaf forests, this parameter is 0.35. Additionally, grasslands are important from several other points of view, such as biodiversity, agricultural production, and tourism, among others [2–4].

A significant portion of Europe's agricultural area is grasslands [5]. The European Union has established the Common Agricultural Policy (CAP) that enables the payment of subsidies to farmers [6]. "Greening" is a measure in the CAP that makes the system of direct payments more environmentally-friendly, requiring the grasslands to be maintained in good agricultural and environmental conditions. One of the obligations of farmers is to maintain their grasslands by mowing or grazing on a yearly basis. National Paying Agencies (NPAs) are required to validate the mowing

requirement to verify subsidy claims. The validation is usually performed by selecting a limited test area, where the checks are then carried out using visual interpretation of very high resolution satellite images and on-site field inspections. The validation process, however, could be made more effective via a more comprehensive use of remote sensing data, especially after the successful launch of the Copernicus program [7]. Use of Earth Observation (EO) data would allow the NPAs to perform the checks over a much larger area, leading to a more effective use of resources and helping to reduce the number of false payments.

Monitoring of agricultural areas has been an important part of remote sensing since the very first EO instruments. Optical remote sensing offers mature methods for the monitoring of agricultural yield [8–10] and management practices [11,12]. However, Whitcraft et al. [13] showed that many important agricultural areas are so persistently and pervasively covered by clouds that less than half of their 8 day composites would be even 70% clear of cloud cover. Authors also concluded that in these areas and time periods, optical polar-orbiting imaging is not likely to be a viable option for operational monitoring. Similarly, laser scanning, while known to be capable of producing reliable vegetation height estimates [14,15], is predominantly applied in the case of forests or bushes, and is too expensive for continuous wide area monitoring. Use of spaceborne synthetic aperture radar (SAR) data would therefore be beneficial, as the SAR signal can penetrate clouds in all but extreme weather conditions, providing continuous data covering a large area.

As in the case of optical remote sensing, investigations of SAR signal attributes in relation to vegetation parameters have been widespread since the first data became available, and research covers different agricultural applications and technical approaches. The launch of Sentinel-1A and -1B SAR satellites now offers an opportunity to investigate agricultural monitoring methods based on regular dense time series of free and open data. Regarding the monitoring of management practices, studies have shown the potential of approaches based on the analysis of backscatter intensities, polarimetric SAR (PolSAR), and interferometric SAR (InSAR). The possibility of detecting harvesting events of sugarcane using backscatter intensities of TerraSAR-X, ASAR/ENVISAT, and PALSAR/ALOS sensors was analysed by Baghdadi et al. [16], who concluded that the events can be detected if the acquisition date is close to the harvesting date and the sugarcane is not dried out before harvesting. In [17], the Radarsat-2 C-band HH/VV (horizontal transmit, horizontal receive/vertical transmit, vertical receive) intensity ratio was shown to be related to the ploughing of winter wheat, but management practices like grazing, mowing, and mixed management on grasslands could not be discriminated. Wang, Ge, and Li [18] analysed the relationship of COSMO-SkyMed X-band, ENVISAT ASAR, and ALOS PALSAR backscatter values to the Normalized Differential Vegetation Index (NDVI), Normalized Difference Water Index (NDWI), and soil moisture index (MI) values without ground truth measurements, and concluded that at paddock scale, X-band HH backscatter could be useful for the detection of grazing or mowing activities on pastures during peak season on non-rainy dates. Mowing events on grasslands were specifically studied using PolSAR by Voormansik et al. in 2013 [19] and 2016 [20], demonstrating that several C-band and X-band polarimetric parameters are sensitive to mowing events in cases where the grass was left on the ground after the event. However, the combination of VV and VH (vertical transmit, horizontal receive) polarized channels offered by the Sentinel-1 means that the PolSAR approach is problematic, as most of the PolSAR methods require fully polarimetric or dual polarimetric co-pol data. Additionally, use of backscatter from one channel (e.g., VV) is problematic, due to variations caused by changing meteorological conditions and vegetation orientation effects [21].

On the other hand, InSAR-based approaches have shown potential for change detection in vegetation, and the regularity of Sentinel-1 data is well-suited for InSAR applications. Early advances in the detection of abrupt changes in vegetation with InSAR were made in the forest domain. In [22], it was shown that clear-cuts have higher interferometric coherence values than forests, in line with observations comparing forested and bare areas in [23]. The approach has been shown to apply for agricultural monitoring as well. High coherence values due to backscattering from the ground were linked to ploughed bare fields and low vegetation height in [24,25]. A similar approach, but for the

detection of mowing events on grasslands, has been studied by Zalite et al. [26,27], where it was demonstrated how 1-day X-band interferometric coherence is much higher for mowed grasslands when compared to grasslands covered by vegetation. However, meteorological effects play an important role in the interpretation of interferometric coherence [28–30], including over bare ground [31]. As one of the sources of change, precipitation may cause temporal decorrelation, complicating interpretation.

The aim of this paper is to describe the relationship between the C-band SAR 12-day repeat pass temporal interferometric coherence and mowing events of grasslands. The study was performed in Central Estonia. We mainly focus on the impact that temporal separation between a mowing event and interferometric acquisitions has on the coherence values. Additionally, we analyse the effect of precipitation on the coherence, as the importance of accounting for meteorological effects in the correct interpretation of this parameter has been previously demonstrated. A more comprehensive understanding of the relationship between coherence and mowing events would allow for the evaluation of the feasibility of using this parameter for future mowing detection applications.

The paper is organised as follows. In Section 2, we present the data used in the study that includes SAR acquisitions, field survey information, and the description of the data processing chain. Section 3 is devoted to presenting the results and discussion about the relationship between the interferometric coherence and mowing events. Additionally, the influence of precipitation on the relationship is analysed. Finally, conclusions are listed in Section 4.

## 2. Materials and Methods

### 2.1. Study Area and Field Measurements

The 6 km × 9 km study area is located in Estonia, in Rannu parish (26°13'10"E, 58°14'17"N), see Figure 1. The area is relatively flat and is predominantly used for agriculture. In total, 37 agricultural grasslands used to grow red clover (*Trifolium pratense* subsp. *sativum*), alfalfa (*Medicago sativa*), timothy-grass (*Phleum pratense*), meadow fescue (*Festuca pratensis*), red fescue (*Festuca rubra*), and other species were used in the experiment. Six grasslands (further as G1 through G6) were monitored from May to September 2015 on a weekly basis, providing information about the vegetation height, wet and dry above-ground biomass, and soil moisture. The measurements were done using the transect method. Ten measurements were taken on a straight line every 25 m. Vegetation height was measured with a measuring tape, and the recorded value represents the height of the majority of vegetation interpreted visually by the field worker. Soil moisture in the upper 5 cm layer was measured using two hand-held conductivity probes: Delta-T ML2x and Extech MO750. All vegetation inside a 0.5 m × 0.5 m square was cut and collected. The vegetation was weighed to measure the wet above-ground biomass. It was then dried and weighed again to provide the dry above-ground biomass.

### 2.2. Mowing Events

On the grasslands used in this study, the grass was mowed to produce fodder. The grass was collected after the mowing event. Mowing events were registered using GPS logs from tractors. The start and end times of each mowing event were recorded. The spatial extent of the event was digitised. In total, 77 mowing events were registered during the 2015 vegetation season. There were 27 events in June, 19 in July, 9 in August, and 22 in September. One grassland could be mowed several times: 38 first, 30 second, and 9 third mows were registered. The size of the mowed area varied between 2.2 ha and 43.2 ha (mean area of 11.9 ha).

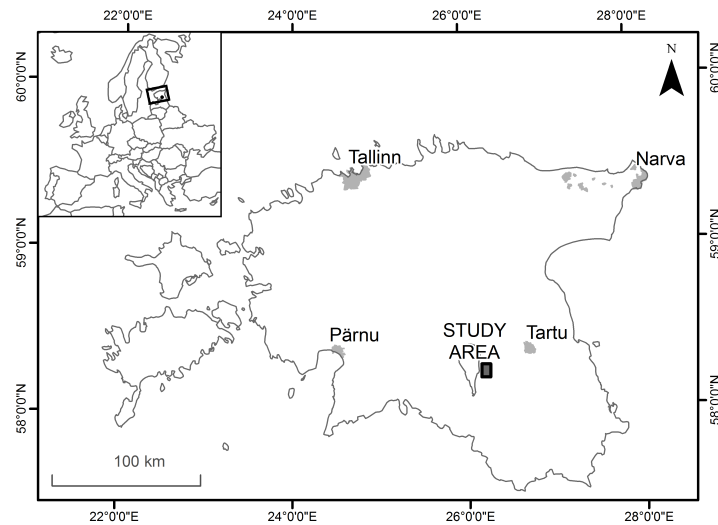


**Figure 1.** Location of the study area in Estonia.

### 2.3. SAR Data

Sentinel-1A is a C-band SAR remote sensing satellite launched into orbit on 3 April 2014. It mostly operates in the Interferometric Wide swath mode (IW) providing dual-pol data (VV + VH). For this study, acquisitions from three geometries (defined by the relative orbit number or RON) were used: R58, R80, and R160. An overview of geometries is given in Table 1. For each geometry, acquisitions in Estonia were made every 12 days, with some exceptions. The data were acquired as Single Look Complex (SLC) products. Precise acquisition dates for each geometry are given in Table 2. The Sentinel-1 orbit maintenance strategy ensures relatively small orbital InSAR baselines on the order of 150 m [32].

**Table 1.** Relative orbit numbers (RONs) used in the study and their parameters [33]. The values are given for the study area. Azimuth (*az*), range (*rg*).

RON	Asc/Desc	Acquisition Time (UTC)	Sub-Swath	Incidence Angle		Ground Range Resolution <i>az</i> × <i>rg</i> , m	
				Near	Far	Near	Far
58	Ascending	16:04	3	44.6	45.0	21.60 × 4.98	21.60 × 4.95
80	Descending	04:34	2	39.0	39.5	21.70 × 4.93	21.70 × 4.87
160	Ascending	15:56	2	37.9	38.4	21.70 × 5.05	21.70 × 4.99

**Table 2.** Acquisition dates for different RONs.

RON	May			June		
58	1	13	25	6	18	30
160	8	20	1	13	25	
80	3	15	27	8	20	
RON	July			August		
58	12	24	5	17	29	
160	7	19	31	12	24	
80	2	14	26	7	19	31
RON	September			October		
58	10		4	16	28	
160	5	17	29	11	23	
80	12	24	6			

#### 2.4. Processing

Processing of the Sentinel-1 images was performed with the SNAP tool (version 2.0.0) provided by the European Space Agency. The SNAP Graph Processing Tool (GPT) was used together with Python 3 to automate the processing workflow. The Sentinel-1 precise orbit files were applied to the scenes. Coregistration to sub-pixel accuracy was done using the S1 TOPS Coregistration function called S1 Back Geocoding. After the coregistration, coherence images were calculated for each image pair according to the procedure outlined in Section 2.5, including the removal of the flat Earth phase term. Terrain correction was done using SRTM 3 sec data and bilinear interpolation, resulting in 4 m × 4 m pixel spacing raster in the European Petroleum Survey Group (EPSG): 3301 coordinate system. Sentinel-1 ground range resolution ranged from 4.87 to 5.05 m within the study area. The 4 m pixel spacing was chosen for the output of the coherence raster, in order to use all of the spatial variation recorded by the sensor. Additionally, backscattering coefficients for VH and VV polarizations were calculated for each of the Sentinel-1 images using the GPT Calibration function.

The field measurements of the six weekly inspected grasslands were averaged to an 80 m × 250 m area surrounding the measurement transect (see Section 2.1). For all field measurement areas involved in the study, the following parameters were calculated from the images over an area defined by the spatial extent of the mowing event for each acquisition date: (1) average VV and VH coherence; and (2) average backscatter values for VV and VH. Additionally, time separation in days between an event and the first acquisition in an interferometric pair was calculated. All of these parameters were recorded for three acquisitions before and three after a mowing event for each geometry. Mowing events' outlines were buffered inside based on the size of the averaging window. This was done in order to exclude pixels that are outside the outline from the calculations. The work flow was automated using the ArcGIS Python package *arcpy*.

#### 2.5. Coherence Estimation

Central to this study is the estimation of the amplitude of the complex correlation coefficient, called coherence. Given two complex SAR images  $s_1$  and  $s_2$  (e.g., Sentinel-1 SLC products), coherence is defined as:

$$\gamma = \frac{|\langle s_1 s_2^* \rangle|}{\sqrt{\langle s_1 s_1^* \rangle \langle s_2 s_2^* \rangle}}, \quad 0 \leq \gamma \leq 1 \quad (1)$$

where  $|\cdot|$  denote the absolute value,  $\langle \cdot \rangle$  denote an averaging operation, and  $*$  denotes the complex conjugate product.

Coherence reaches the maximum value of 1 when the position and physical properties of the scatterers within the averaging window  $\langle \cdot \rangle$  are the same for both images  $s_1$  and  $s_2$ . On the other hand, changes in the position or properties of the scatterers cause the coherence value to decrease. Additionally, a decrease of the coherence value or decorrelation can be caused by a mismatch in the properties of the two imaging systems involved caused by volume scattering, processing errors, and others—a full list is presented in [34]. These sources, however, are negligible in the context of this study (including volume decorrelation, given the relatively small baselines between interferometric acquisitions). Instead, we focus on temporal decorrelation. It is caused by changes in the scatterers over time; i.e., between the acquisitions. In the presence of vegetation, temporal decorrelation decreases the measured coherence. On the other hand, when the vegetation is removed, temporal decorrelation is expected to be lower due to a more coherent scattering from the soil, increasing the measured coherence. In order to evaluate the temporal decorrelation term that could indicate a mowing event, additional decorrelation sources have to be taken into account. The estimated coherence  $\gamma_{total}$  can be defined as:

$$\gamma_{total} = \gamma_{temporal} \gamma_{SNR} \gamma_{bias} \gamma_{other} \quad (2)$$

where  $\gamma_{total}$  is the calculated coherence from Equation (1),  $\gamma_{temporal}$  is the temporal decorrelation,  $\gamma_{SNR}$  is decorrelation due to system noise (SNR: signal-to-noise ratio),  $\gamma_{bias}$  is influenced by the size of the averaging window, and  $\gamma_{other}$  are the other terms mentioned before as being negligible. Procedures for the evaluation of  $\gamma_{SNR}$  and  $\gamma_{bias}$  decorrelation terms are given in the following subsections.

### 2.5.1. SNR Decorrelation

$\gamma_{SNR}$  is caused by thermal noise of the system. In most cases, when the signal-to-noise ratio is higher than 10 dB, this decorrelation term can be ignored. However, due to the relatively weak interaction between grassland vegetation and the C-band signal, this term is not negligible in this study and has to be taken into account.  $\gamma_{SNR}$  is defined as [35]:

$$\gamma_{SNR} = \frac{1}{\sqrt{\left(1 + \frac{1}{SNR_{sat1}}\right) \left(1 + \frac{1}{SNR_{sat2}}\right)}} \quad (3)$$

where  $SNR_{sat}$  is calculated for each of the two images in the interferometric pair according to:

$$SNR_{sat} = \frac{\sigma_{sat}^0 - NESZ_{sat}}{NESZ_{sat}} \quad (4)$$

where  $\sigma_{sat}^0$  is the backscattering coefficient of the area under investigation in the respective acquisition, and  $NESZ_{sat}$  is a range-dependent noise parameter that can be calculated using look-up tables provided in the Sentinel-1 metadata. The parameters in Equation (4) are in linear scale.

In this study, the mean  $\gamma_{SNR}$  value for VH acquisitions was 0.91, and was 0.98 for VV. The minimum values were 0.66 for VH and 0.94 for VV.

### 2.5.2. Estimation Bias

Estimation of coherence is biased towards higher values, decreasing the contrast between areas of varying low coherence [36]. The bias can be decreased by using larger averaging windows in Equation (1). The choice of window sizes, however, has to be balanced with image resolution and, in this case, size of the grasslands. In this study, we used averaging windows with the following sizes (azimuth (az)  $\times$  range (rg)):  $5 \times 21$  for R58,  $5 \times 19$  for R80, and  $5 \times 19$  for R160, producing a footprint on the ground of  $\approx 71 \text{ m} \times 69 \text{ m}$  for all geometries. This resulted in the equivalent number of looks (ENL) of 50 for R58, and 46 for R80 and R160. The number of ENLs ensured that coherence estimated using the aforementioned window sizes was not heavily biased, with the bias value of 0.14–0.15 given true coherence of 0.

## 2.6. Precipitation Data

In the study carried out by Zalite et al. [27], it was shown that precipitation can hinder the detection of mowing events when using a similar approach to that employed in this research. In order to investigate the effect precipitation has on temporal coherence, precipitation amounts before the images in the first interferometric pair after the mowing events were estimated using a DualPol weather radar located in Sürgavere, 50 km to the north–west of the study area. The weather radar was produced by Vaisala Group, and it operates in the C-band (wavelength of 5.33 cm).

The Estonian Weather Service provided 15-minute scan files which were processed with the *wradlib* Python package (Heistermann et al. [37]) to produce pseudo constant altitude plan position indicator (PseudoCAPPI) estimates in the height of 500 m. Using the 15 min interval PseudoCAPPI estimates, accumulated rainfall maps at  $300 \text{ m} \times 300 \text{ m}$  spatial resolution were computed for 1 h, 3 h, 6 h, 12 h, and 24 h before the Sentinel-1 acquisitions. Precipitation estimates for each of the fields were

created by averaging those 300 m × 300 m pixels whose centre intersected with the spatial extent of the mowing event. The accuracy of precipitation estimates was assessed by comparing 1-h estimates larger than 0.10 mm with hourly measurements (259 measurements with an average of 1.1 mm and a maximum of 9.5 mm) in Tõravere meteorological station (15 km to the east of the study area) over the period from May to September 2015. The coefficient of determination  $R^2$  was 0.67 and Root Mean Squared Error (RMSE) was 0.95. Comparing the accuracy of precipitation estimates to the results from Kirstetter et al. [38], it was concluded that our estimates are accurate enough to be used in this study.

Precipitation amounts can show great spatial variability. For example, Tõravere meteorological station did not register any precipitation between 13:00 to 16:00 UTC on 31 July, while precipitation estimates indicated 1.4 mm precipitation over the measurement areas. By using the estimates from the weather radar, we aimed to take this spatial variability into account.

Precipitation estimates for three image pairs before and three after a mowing event were used to analyse the effect precipitation has on coherence values. The *matplotlib* Python package [39] was used for visualisation.

### 3. Results and Discussion

Coherence values for each of the six measurement areas where vegetation parameters were recorded throughout the summer are given in Figures 2 and 3 for VH and VV polarisations, respectively. These time series illustrate the complexity of the relationship between mowing events and coherence. First of all, a mowing event was rarely characterised by the complete removal of vegetation, and grass with height of 0.1 to 0.2 m was often left on the field. Thus, very high coherence caused by coherent scattering from soil was rarely observed. Even when bare soil was present (G1 in May, and G3/G4 at the end of August), coherence values fluctuated. In the case of G1, low VV coherence ( $\gamma_{vv}$ ) in the presence of bare soil was recorded in the middle of May. It was likely caused by farming activity visible on the field survey photos. For G3/G4, after the complete removal of vegetation in August, the grasslands were subjected to further farming activities, causing coherence to remain rather low.

In the presence of vegetation, coherence values were also rather varied. However, some changes were apparent, and could be linked to mowing events. For example, R160  $\gamma_{vv}$  increased from 0.15 to 0.47 for G5 after a mowing event on 6 June. Figure 4 illustrates the increase of coherence after this event. To a lesser extent,  $\gamma_{vv}$  increased from 0.18 to 0.34 for the same grassland after an event on 3 August. For the same events, R58  $\gamma_{vv}$  changed from 0.16 to 0.27 and from 0.24 to 0.38. The increase of coherence was mostly not so apparent for other grasslands that were inspected weekly. In the case of G6, the responses to an event in 8 June and 9 June were weak: R160  $\gamma_{vv}$  increased from 0.15 to 0.23 and R58 from 0.19 to 0.22. Response from R58 was probably influenced by rain—the 3-h precipitation estimate before the 18 June acquisition was 0.5 mm. The second mowing on 17 July was followed by a slight increase in R160 and R58  $\gamma_{vv}$ . The R160  $\gamma_{vv}$  value, however, might have been decreased by precipitation, as the 3-h precipitation estimate before the 21 July acquisition was 1.3 mm. R80's  $\gamma_{vv}$  value also increased, from 0.14 to 0.27 for G4 after an event in mid July, while R160 coherence was severely influenced by rain.

Weaker responses could be observed in the cases of G1 and G2. An increase of  $\gamma_{vv}$  was recorded after an event in July when R160 increased from 0.17 to 0.23 (G1) and R58 increased from 0.14 to 0.24 (G2). For other events, precipitation might have mitigated the increase. Precipitation estimates indicated rain in the case of the 21 July/12 August pair for G1, and the 19 July/31 July and 31 July/12 August pairs for G2. For both fields,  $\gamma_{vv}$  remained low in the beginning of August, possibly because of plant growth. The 12 August/24 August coherence was low for G1 and G2, and field survey data indicated that grass had grown by about 30 cm on G1 and by 10 cm on G2 between the image pair acquisitions. This indicates that the 12-day repeat pass configuration is not temporally dense enough for the mowing detection in the case of rapidly growing vegetation.

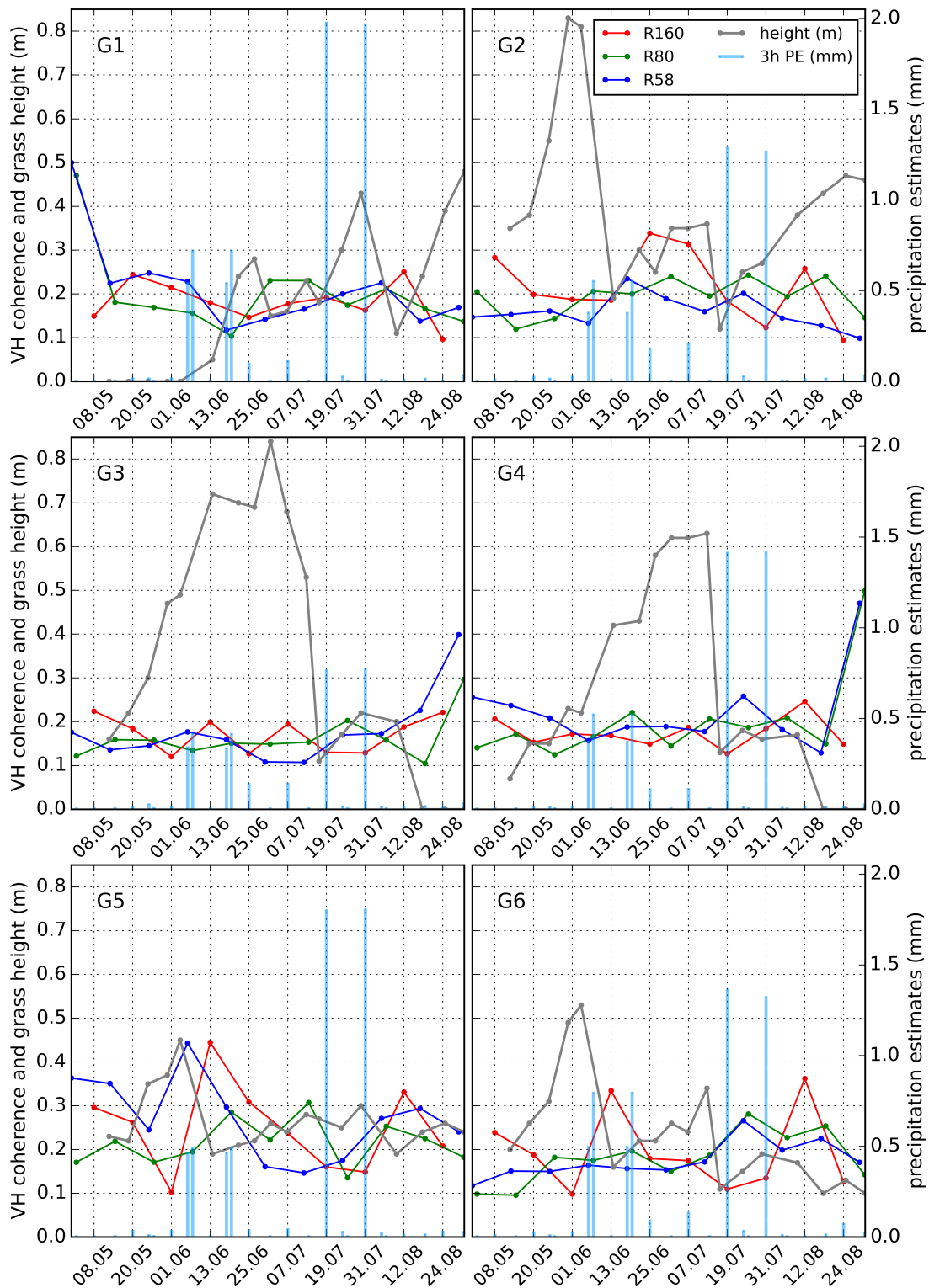


**Figure 2.** The 2015 time series of recorded height and coherence values for grasslands where the field survey was conducted. Polarization is vertical transmit, horizontal receive (VH). Date of the first image of the coherence pair is given on the x-axis. Vertical blue lines indicate the sum of 3-h precipitation estimates (PE) in mm for the image pair.

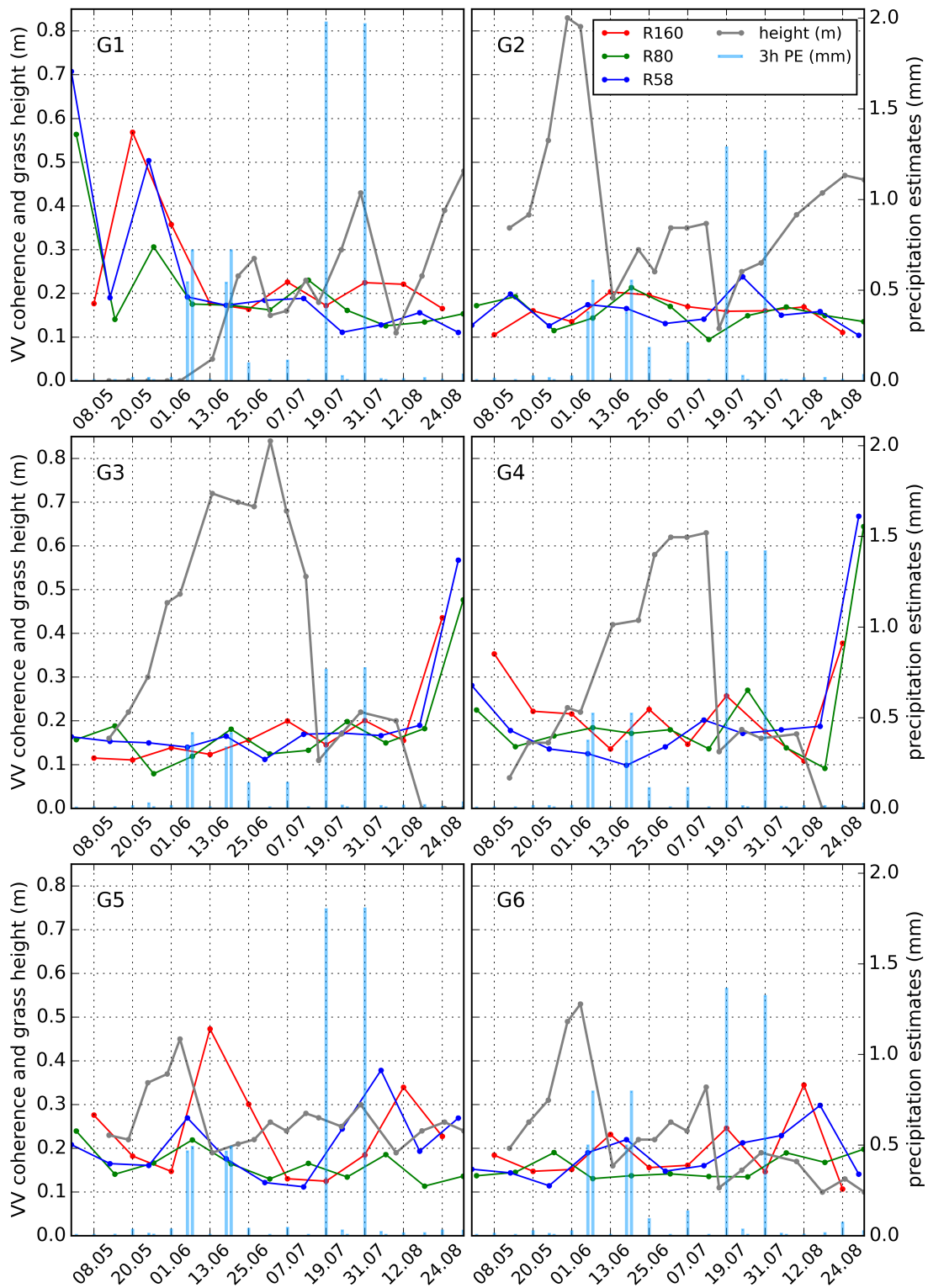


**Figure 3.** The 2015 time series of recorded height and coherence values for grasslands where the field survey was conducted. Polarization is vertical transmit, vertical receive (VV). Date of the first image of the coherence pair is given on the x-axis. Vertical blue lines indicate the sum of 3-h precipitation estimates (PE) in mm for the image pair.

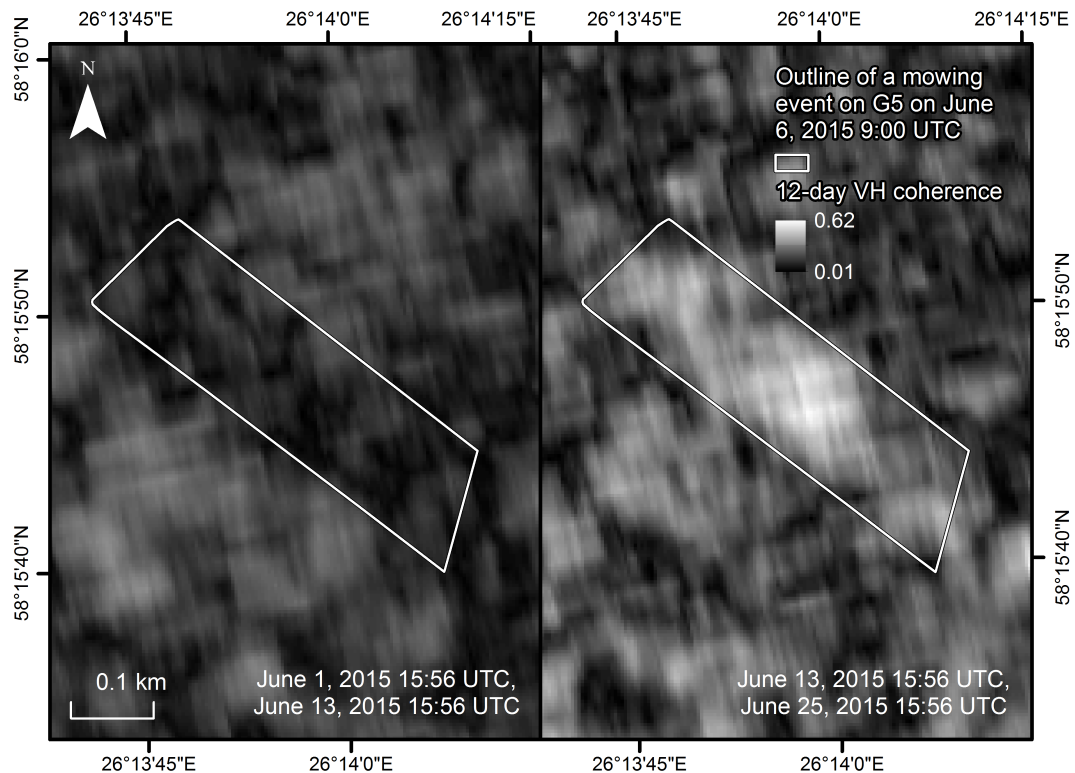


**Figure 4.** Sentinel 1A 12-day VH coherence before (left) and after (right) a mowing event on G5 on 6 June 2015.

The stronger response to mowing on G5 could be partially explained by the vegetation structure present on the grassland. The soil had a rather large moisture content (>50% soil moisture vs. <30% for other grasslands), and the grass was sparse, with lower wet above-ground biomass (AGB) values (e.g., 2.1 for G1, 4.1 for G3, and 1.6 for G5 in  $\text{kg}/\text{m}^2$  at the peak of the season). The sparseness of vegetation would cause more coherent backscatter from the soil, especially after partial removal of vegetation, resulting in higher coherence values. G5 was the only grassland where weak relation between soil moisture and coherence measurements was detected, with  $R^2 = 0.25$  for  $\gamma_{vh}$  and  $R^2 = 0.56$  for  $\gamma_{vv}$ .

After a mowing event on G3 in the middle of July, the increase of coherence values was small. Low coherence values computed from the R58 24 July/5 August image pair could be caused by the specific mowing method used. Grass was mowed above  $\approx 30$  cm to harvest the seeds, and the remaining straws were pressed to the ground. The biomass that was left on the ground decreased the portion of backscatter coming from the soil and led to lower coherence values. Additionally, the positions of these long straws could be changed by the wind between the acquisitions, thereby decreasing the coherence. Furthermore, R160 acquisitions were most probably also influenced by rain. Conversely, several polarimetric studies have reported higher sensitivity to harvesting events when vegetation was left on the ground after an event [19,20,40].

Differences could also be observed between the results for VV and VH. The response of VH coherence ( $\gamma_{vh}$ ) was rather different from that of  $\gamma_{vv}$  for G1 in May and the beginning of June—values of  $\gamma_{vh}$  were much smaller, by 0.2–0.3 units, ranging across all geometries. In the case of G2, R160  $\gamma_{vh}$  reached >0.30 in July, while  $\gamma_{vv}$  remained under 0.20. Further differences in response could be observed for G5:  $\gamma_{vv}$  0.27 vs.  $\gamma_{vh}$  0.44 for R58 6 June/18 June image pair, and  $\gamma_{vv}$  0.38 vs.  $\gamma_{vh}$  0.27 for R58 5 August/17 August image pair, as well as for G6:  $\gamma_{vv}$  0.23 vs.  $\gamma_{vh}$  0.33 for R160 16 June/25 June image pair, and  $\gamma_{vv}$  0.13 vs.  $\gamma_{vh}$  0.28 for R80 26 July/7 August image pair. The divergences could have been caused by differences in scattering due to soil roughness and vegetation structure. For example,

the VV backscatter for G1 in May (bare soil) was on average 10 dB higher than VH, with VH values dropping as low as  $-24$  dB, reaching close to the noise-equivalent sigma zero (NESZ) value of  $-28$  dB.

Easily observable differences existed between  $\gamma_{vv}$  and  $\gamma_{vh}$  values of different RONS. These could be explained by the difference in acquisition times, with conditions on the grasslands varying rapidly when the vegetation is growing. An additional source of decorrelation was likely the morning dew, as morning acquisitions (R80) produced consistently lower coherence values on average. The varying dew conditions can cause variation in the position of scatterers in a scene, thus decreasing coherence. The R58 geometry, on the other hand, might have resulted in lower coherence values on average, due to shallower incidence angles (for the middle of the study area, the incidence angles were  $38.2^\circ$  for R160,  $44.8^\circ$  for R58, and  $39.3^\circ$  for R80). This is in contrast to polarimetric approaches for harvest detection, where shallower incidence angles are often preferred [41].

The observed differences in coherence responses after mowing events could be caused by several factors, such as soil roughness and moisture, species composition, and precipitation (or intercepted moisture). Additionally, time separation between a mowing event and first acquisition of the InSAR pair has to be taken into account. In the following two subsections, we analyse the impact of precipitation and time separation on the measured coherence in cases when a mowing event is known to have happened. These analyses will help to understand the general effects regardless of specific knowledge about species and soil conditions.

### 3.1. Effect of Precipitation

Analysis of the precipitation estimates results revealed that 3-h precipitation estimates described the interactions between the coherence and precipitation similarly to those of 1, 6, 12, and 24 h estimates. One reason for that could be the limited number of image pair samples available within 12 days after a mowing event. Larger variation between 1 to 24 h estimates might have been observed, given more data. On the other hand, the precipitation can dry out rather quickly, depending on the temperature on the grassland. The optimal time window length before the image acquisitions has to be analysed with a more extended sample size of mowing events. Given the similarity of the precipitation estimates of different time periods, only 3-h precipitation estimates were further used in this study.

The relationship of coherence and 3-h precipitation estimates for the first image pair after a mowing event is shown in Figure 5. When precipitation estimates were over 0.25 mm,  $\gamma_{vv}$  and  $\gamma_{vh}$  remained under 0.25 after a mowing event with a few exceptions, and  $\gamma_{vv}$  had slightly higher values than  $\gamma_{vh}$ . For further analysis, coherence values were divided into groups with 3-h precipitation estimates  $\leq 0.25$  mm and  $>0.25$  mm. A threshold of 0.25 mm was chosen because it allowed all three image acquisition geometries to be divided into two groups based on 3-h precipitation estimate values, and these two groups can likely be associated with rain and rain-free conditions on the grasslands. Figure 6 shows that the medians of R160 VH and VV coherence in these two groups differ significantly. Precipitation up to 3-h before one or both of the image acquisitions changes the structure and dielectric constant of the vegetation on grassland, remarkably decreasing the coherence. Loss of coherence due to precipitation has also been reported by Zalite et al. [27] and Ahmed et al. [42]. At the same time, R58 and R80 geometries did not show any significant differences—the notches around the median that represent 95% confidence intervals are overlapping. The 3-h precipitation estimate values were quite small before R80 and R58 acquisitions, and they might not have significantly affected the coherence. Additionally, the accuracy of the precipitation estimates has to be considered, as well as the small sample size. For R80, the median VH and VV coherence values were lower than 0.2 for the precipitation estimates  $\leq 0.25$  mm groups, so the drop of coherence could not be large for the precipitation estimates  $>0.25$  mm group. The differences between VV and VH for this analysis were not significant.

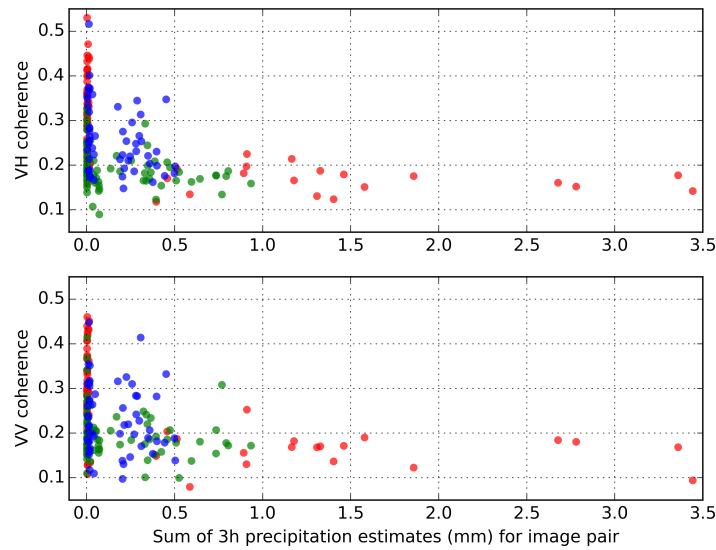


**Figure 5.** Scatterplot of coherence values and the sum of 3-h precipitation estimates at 300 m × 300 m spatial resolution based on weather radar data for the first image pair available within 12 days after a mowing event. R160 is represented by red, R80 by green, and R58 by blue dots.

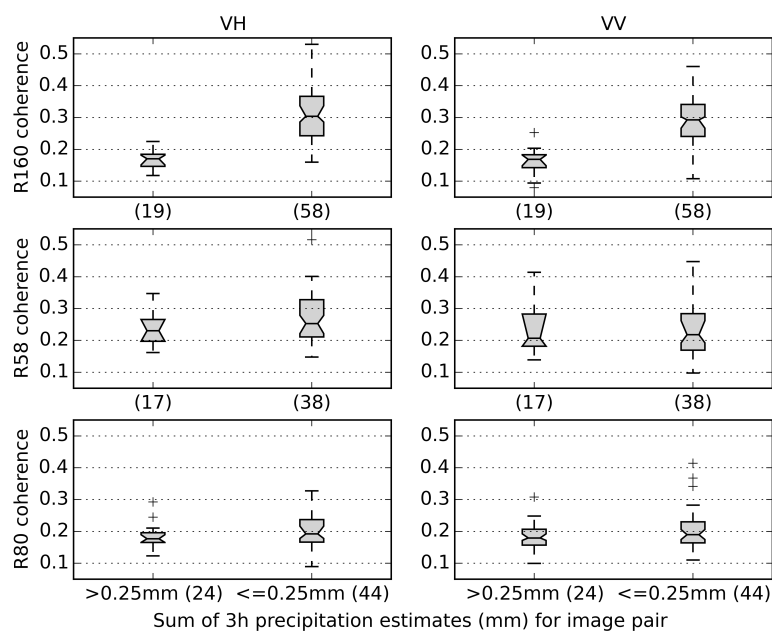


**Figure 6.** Box plots comparing coherence values for two groups—where the sum of 3-h precipitation estimates was  $>0.25$  and  $\leq 0.25$  mm. Group sizes are given in parenthesis. Coherence values and the sum of precipitation estimates are calculated for first image pair within 12 days after a mowing event. The box extends to first (Q1) and third (Q3) quartile values, the whiskers extend to 1.5 times interquartile range ( $IQR = Q3 - Q1$ ) from the box (e.g.,  $Q1 - 1.5 \times IQR$ ), beyond the whiskers, data points are considered outliers. The notches around the median represent 95% confidence intervals calculated with 5000 bootstrap cycles.

### 3.2. Dependence on Time Separation

A decreasing trend in coherence values before a mowing event and an increase after it could be observed. These trends are presented in Figure 7. In the case of rain, the coherence rarely exceeded 0.25. There were no clear gaps in the time separation values, indicating that there were enough samples to investigate the relationship between the coherence and time separation from a mowing event.

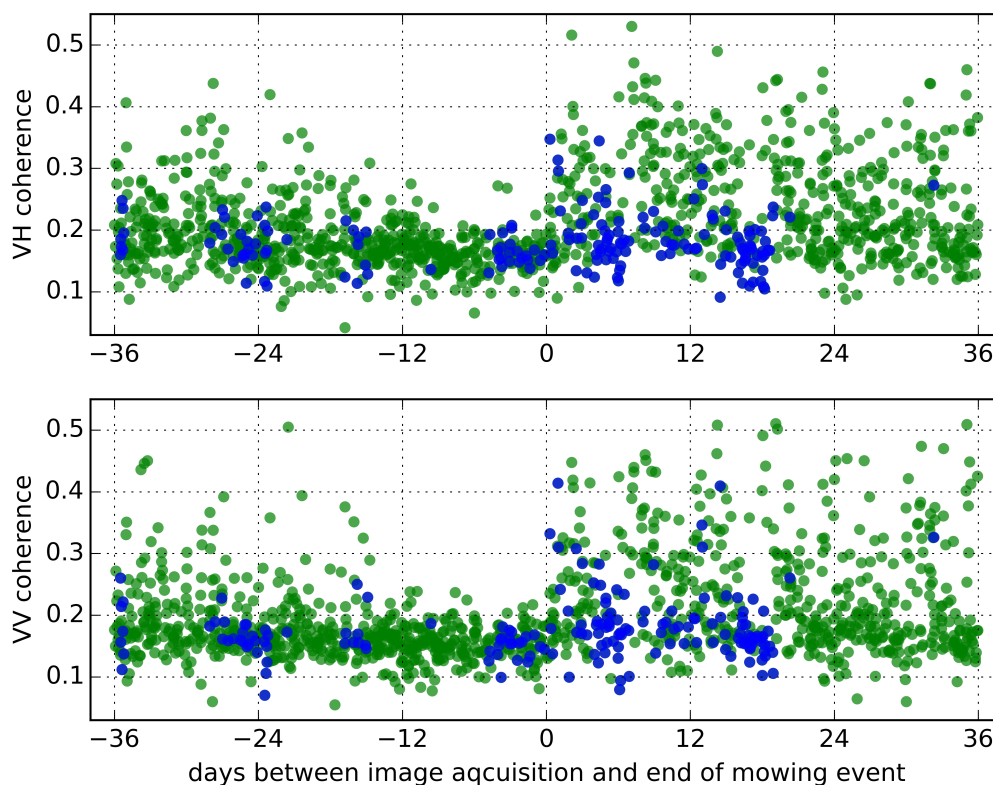


**Figure 7.** Scatterplot of coherence values and time separation between the first image acquisition in coherence pair and a mowing event. Blue dots mark the coherence values with 3-h precipitation estimates  $>0.25$  mm.

The coherence values were divided into six 12-day interval groups based on the time separation to investigate the changes in coherence (Table 3). Not all of the 12-day repeat-pass acquisitions for R80 and R58 were available, thus twelve time separation groups out of eighteen had coherence measurements for all 77 mowing events. Precipitation filtering based on precipitation values  $>0.25$  mm had the highest influence on the number of samples for R80, where 16% (R160 13%, R58 10%) of the samples were removed.

**Table 3.** Time groups used in the time separation analysis. The range defines days before the mowing event (−) or after the event (+). The R58, R80, and R160 columns contain the number of samples for each group and their respective geometries. The number of samples after precipitation filtering is also given in parenthesis.

Group	Range	R58	R80	R160
T−3	−36... −24	77 (69)	77 (61)	77 (77)
T−2	−24... −12	77 (77)	77 (70)	77 (67)
T−1	−12... 0	63 (56)	77 (71)	77 (67)
T+1	0... +12	55 (38)	77 (53)	77 (58)
T+2	+12... +24	69 (59)	68 (50)	77 (57)
T+3	+24... +36	77 (77)	55 (55)	77 (76)

Results show that T+1, T+2, and T+3 median  $\gamma_{vv}$  and  $\gamma_{vh}$  values were statistically significantly higher compared to group T−1 (Figure 8). The exact median values for the time separation groups and differences between them are given in Table 4 for VH and in Table 5 for VV. The mowing event influenced median  $\gamma_{vv}$  and  $\gamma_{vh}$  values significantly, even after 24 to 36 days after the mowing event. The only exception in the data set was the morning acquisition geometry R80  $\gamma_{vv}$  T+3<sub>R80</sub> group, for

which the median was not significantly different from the  $T-1_{R80}$  group median. Increase of coherence after a mowing event is in line with a similar previous study that was based on X-band data and 1-day interferometric pairs [27]. In contrast to that study, the use of C-band in this experiment might have ensured that the coherence values were statistically significantly higher for a period of up to 36 days after an event.

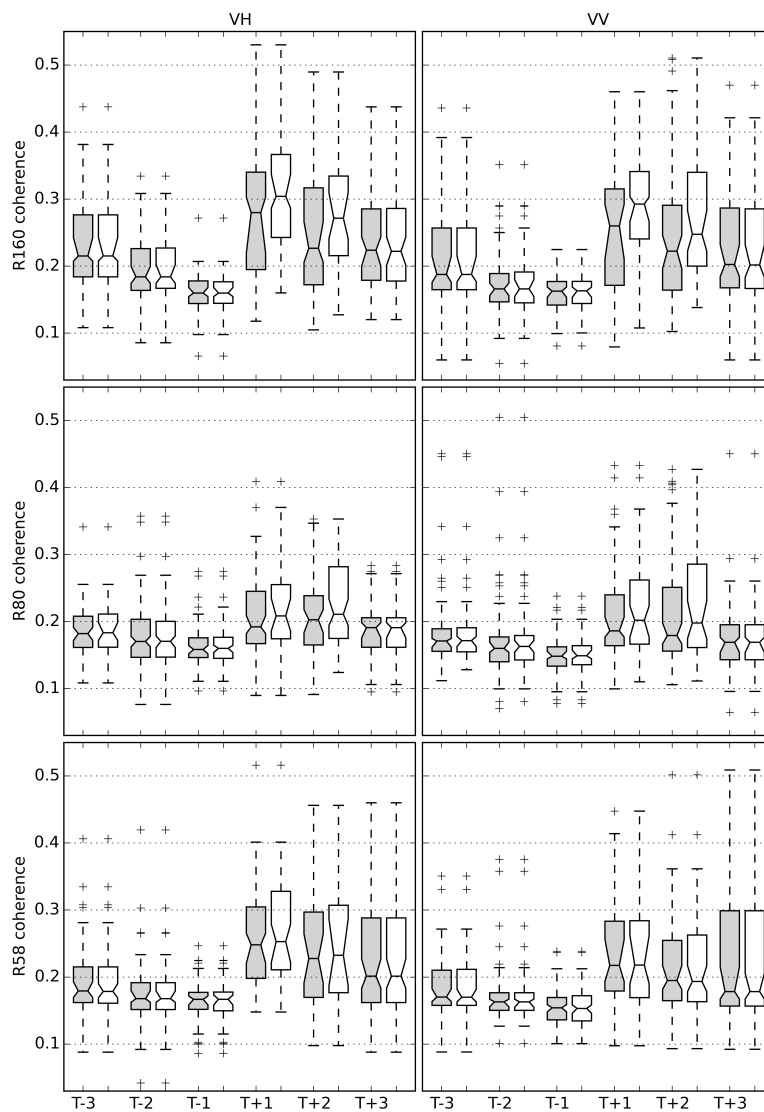


**Figure 8.** Boxplots of coherence and time separation from a mowing event. Grey boxplots represent unfiltered data, while white boxplots represent the precipitation filtered data.

**Table 4.** Median coherence values for time separation groups and VH polarisation. Values without parentheses indicate unfiltered data, while precipitation filtered data is given in parenthesis.

RON	T-1	T+1	T+2	T+3	(T+1)-(T-1)	(T+2)-(T-1)	(T+3)-(T-1)
R160	0.16 (0.16)	0.28 (0.30)	0.23 (0.27)	0.22 (0.22)	0.12 (0.14)	0.067 (0.11)	0.064 (0.062)
R58	0.17 (0.17)	0.25 (0.25)	0.23 (0.23)	0.20 (0.20)	0.081 (0.086)	0.061 (0.066)	0.035 (0.035)
R80	0.16 (0.16)	0.19 (0.21)	0.20 (0.21)	0.19 (0.19)	0.034 (0.048)	0.044 (0.051)	0.033 (0.031)

**Table 5.** Median coherence values for time separation groups and VV polarisation. Values without parentheses indicate unfiltered data, while precipitation filtered data is given in parenthesis.

RON	T-1	T+1	T+2	T+3	(T+1)-(T-1)	(T+2)-(T-1)	(T+3)-(T-1)
R160	0.16 (0.16)	0.26 (0.29)	0.22 (0.25)	0.20 (0.20)	0.097 (0.13)	0.060 (0.085)	0.040 (0.039)
R58	0.15 (0.15)	0.22 (0.22)	0.19 (0.19)	0.18 (0.18)	0.063 (0.065)	0.041 (0.040)	0.024 (0.025)
R80	0.15 (0.15)	0.19 (0.20)	0.18 (0.20)	0.17 (0.17)	0.038 (0.053)	0.031 (0.049)	0.021 (0.020)

The T+1 group gave the best separation between the mowed and not mowed grasslands. In most cases, the upper quartile of the T-1 group and the lower quartile of the T+1 group did not overlap. The difference in median values for T-1 and T+1 groups was smallest for the R80 morning pass geometry. Even after the mowing, coherence values stayed close to 0.20. This was most probably caused by dew, which can decrease the coherence, as it affects the dielectric constant that shapes the backscattering intensities of grass and also the reflection properties in the vegetation layer, thus influencing the phase. The lowest coherence could be expected when one of the images in the coherence pair was taken in dew conditions and the other in dry conditions. Even when both images were taken in the dew conditions, the spatial distribution of water drops in the vegetation layer was most probably random, leading to low coherence values.

Variation of coherence was lower for T-3, T-2, and T-1 groups compared to T+1, T+2, and T+3 groups. Temporal decorrelation caused by tall grass decreases coherence values close to the noise floor. On the other hand, the decorrelation caused by the movement of plants was much smaller for shorter grass. In this case, other effects, such as weather conditions and human activities make the coherence much more variable. The medians of groups T-3 and T+3 are not significantly different.

Taking into account R160 and R58 geometries, the average difference between precipitation filtered T-1<sub>R160,R58</sub> median compared to T+1<sub>R160,R58</sub>, T+2<sub>R160,R58</sub>, and T+3<sub>R160,R58</sub> groups is 0.084 for  $\gamma_{vh}$  and 0.064 for  $\gamma_{vv}$ . Therefore, VH polarisation might have a slightly better ability to detect mowing events. On average, the confidence interval for VH median at the 95% confidence level is 0.035, and for VV median it is 0.031. A similar outcome has been observed in studies focused on the use of SAR backscatter for agricultural monitoring. Hajj et al. [43] reported that the X-band HV polarisation is more sensitive to grasslands parameters than HH. Additionally, Baghdadi et al. [16] concluded that the co-pol channels (HH and VV) have a slightly lower potential for the detection of the sugarcane harvest.

Taking into account all three image acquisition geometries, precipitation filtering affected the T+1, T+2, and T+3 groups more than the T-1, T-2, and T-3 groups. For T-1, T-2, and T-3, the average difference in medians between filtered and unfiltered data was under 0.10%. At the same time, the average difference for T+1, T+2, and T+3 groups was 4.9%. High vegetation decorrelates both in dry and wet conditions; thus, the removal of events with precipitation has little effect for T-1, T-2, and T-3 groups. The median values of precipitation filtered and unfiltered groups were not statistically significantly different. The influence of precipitation filtering on separation between T-1 and T+1/T+2/T+3 can be evaluated from Tables 4 and 5, where the coherence values after filtering are given in parenthesis.

#### 4. Conclusions

In this paper, 12-day repeat pass Sentinel-1 interferometric coherence calculated for three acquisition geometries was analysed in relation to mowing events recorded on agricultural grasslands in Central Estonia over the vegetative season of 2015. Results showed that after a mowing event, median  $\gamma_{vv}$  and  $\gamma_{vh}$  values were statistically significantly higher when compared to pre-event values. The group containing coherence measurements from 0 to 12 days after a mowing event gave the best separation between mowed and not mowed grasslands. The coherence was higher even 24 to 36 days after a mowing event when compared to values from not mowed measurements. The increase of coherence for the VH polarisation was higher than for the VV polarisation.

Several factors impeded the increase of coherence after a mowing event. The factors were farming activities, such as sowing or ploughing, height of the cut, rapid growth of grass, and precipitation before image acquisitions. In the future, 6-day pairs consisting of Sentinel-1A and 1B acquisitions should alleviate some of these factors.

However, use of C-band SAR repeat pass interferometric coherence for mowing detection is feasible. The aforementioned factors that introduce ambiguities in event detection could be addressed by including ancillary data in the analysis. Further research should reveal how various farming methods, soil types, soil moisture, relative humidity, strong winds, topography, and grassland species influence the relationship between coherence and mowing. The accuracy of mowing detection using various estimation methods should be analysed. For instance, NPAs could possibly use these findings to optimise the work of validating the mowing requirement set by the European Union CAP. Additionally, the results may be beneficial for a general service for classification of management practises in agricultural areas.

**Acknowledgments:** This study was supported by grant no. IUT2-16 of the Ministry of Education and Science of Estonia. Authors appreciate the help from Aleksei Vastenko and Tanel Voormansik with weather radar precipitation estimates, Estonian Weather Services for providing weather radar and meteorological station data, Rait Hallimäe for providing GPS logs from mowing tractors, and Madis Ajaots and Rait Hallimäe for allowing measurement campaign to be carried out on their grasslands.

**Author Contributions:** Tanel Tamm, Karlis Zalite and Kaupo Voormansik conceived and designed the experiments; Kaupo Voormansik, Karlis Zalite, Liina Talgre and Tanel Tamm designed and conducted the field survey; Tanel Tamm performed the experiments; Tanel Tamm and Karlis Zalite analysed the data; Tanel Tamm and Karlis Zalite wrote the great majority of the paper.

**Conflicts of Interest:** The authors declare no conflict of interest.

## Abbreviations

The following abbreviations are used in this manuscript:

az	azimuth
CAP	Common Agricultural Policy
ENL	equivalent number of looks
EO	earth observation
EPSG	European Petroleum Survey Group
DualPol	dual-polarization
GPP	gross primary production
GPT	SNAP Graph Processing Tool
InSAR	interferometric SAR
IQR	interquartile range
IW	interferometric wide swath mode
MI	soil moisture index
NDVI	Normalized Differential Vegetation Index
NDWI	Normalized Difference Water Index
NESZ	Noise-Equivalent Sigma Zero
NPA	National Paying Agency
NPP	net primary production
PolSAR	polarimetric SAR
PseudoCAPPI	pseudo constant altitude plan position indicator
Q1	first quartile
Q3	third quartile
rg	range

RON	relative orbit number
SAR	synthetic aperture radar
SLC	single look complex
SNAP	Sentinel application platform
SNR	signal-to-noise ratio
UTC	coordinated universal time
VH	vertical transmit, horizontal receive
VV	vertical transmit, vertical receive

## References

- Zhao, M.; Heinsch, F.A.; Nemani, R.R.; Running, S.W. Improvements of the MODIS terrestrial gross and net primary production global data set. *Remote Sens. Environ.* **2005**, *95*, 164–176.
- Gibon, A. Managing grassland for production, the environment and the landscape. Challenges at the farm and the landscape level. *Livest. Prod. Sci.* **2005**, *96*, 11–31.
- Hopkins, A.; Holz, B. Grassland for agriculture and nature conservation: Production, quality and multi-functionality. *Integrating Effic. Grassl. Farming Biodivers.* **2005**, *10*, 15–29.
- Watkinson, A. Grasslands, grazing and biodiversity: Editors' introduction. *J. Appl. Ecol.* **2001**, *38*, 233–237.
- Smit, H.; Metzger, M.; Ewert, F. Spatial distribution of grassland productivity and land use in Europe. *Agric. Syst.* **2008**, *98*, 208–219.
- Gray, J. The common agricultural policy and the re-invention of the rural in the European community. *Sociol. Rural* **2000**, *40*, 30–52.
- Copernicus Program. Available online: <http://copernicus.eu> (accessed on 20 May 2016).
- Moran, M.S.; Inoue, Y.; Barnes, E.M. Opportunities and limitations for image-based remote sensing in precision crop management. *Remote Sens. Environ.* **1997**, *61*, 319–346.
- Moulin, S.; Bondeau, A.; Delecolle, R. Combining agricultural crop models and satellite observations: From field to regional scales. *Int. J. Remote Sens.* **1998**, *19*, 1021–1036.
- Meroni, M.; Marinho, E.; Sghaier, N.; Verstrate, M.M.; Leo, O. Remote sensing based yield estimation in a stochastic framework—Case study of durum wheat in Tunisia. *Remote Sens.* **2013**, *5*, 539–557.
- Fuller, D.O. Trends in NDVI time series and their relation to rangeland and crop production in Senegal, 1987–1993. *Int. J. Remote Sens.* **1998**, *19*, 2013–2018.
- Sakamoto, T.; Yokozawa, M.; Toritani, H.; Shibayama, M.; Ishitsuka, N.; Ohno, H. A crop phenology detection method using time-series MODIS data. *Remote Sens. Environ.* **2005**, *96*, 366–374.
- Whitcraft, A.K.; Vermote, E.F.; Becker-Reshef, I.; Justice, C.O. Cloud cover throughout the agricultural growing season: Impacts on passive optical earth observations. *Remote Sens. Environ.* **2015**, *156*, 438–447.
- Nakajima, T. Estimating tree growth using crown metrics derived from LiDAR data. *J. Indian Soc. Remote Sens.* **2016**, *44*, 217–223.
- Rybansky, M.; Brenova, M.; Cermak, J.; van Genderen, J.; Sivertun, Å. Vegetation structure determination using LIDAR data and the forest growth parameters. In Proceedings of the IOP Conference Series: Earth and Environmental Science, Kuala Lumpur, Malaysia, 13–14 April 2016; IOP Publishing: Tokyo, Japan, 2016; Volume 37.
- Baghdadi, N.; Boyer, N.; Todoroff, P.; El Hajj, M.; Begue, A. Potential of SAR sensors TerraSAR-X, ASAR/ENVISAT and PALSAR/ALOS for monitoring sugarcane crops on Reunion Island. *Remote Sens. Environ.* **2009**, *113*, 1724–1738.
- Dusseux, P.; Corpetti, T.; Hubert-Moy, L.; Corgne, S. Combined use of multi-temporal optical and radar satellite images for grassland monitoring. *Remote Sens.* **2014**, *6*, 6163–6182.
- Wang, X.; Ge, L.; Li, X. Pasture monitoring using SAR with COSMO-SkyMed, ENVISAT ASAR, and ALOS PALSAR in Otway, Australia. *Remote Sens.* **2013**, *5*, 3611–3636.
- Voormansik, K.; Jagdhuber, T.; Olesk, A.; Hajnsek, I.; Papathanassiou, K.P. Towards a detection of grassland cutting practices with dual polarimetric TerraSAR-X data. *Int. J. Remote Sens.* **2013**, *34*, 8081–8103.
- Voormansik, K.; Jagdhuber, T.; Zalite, K.; Noorma, M.; Hajnsek, I. Observations of cutting practices in agricultural grasslands using polarimetric SAR. *IEEE J. Sel. Top. Appl. Earth Obs. Remote Sens.* **2015**, *9*, 1382–1396.

21. Bouman, B.A.; van Kasteren, H.W. Ground-based X-band (3-cm wave) radar backscattering of agricultural crops. II. Wheat, barley, and oats; the impact of canopy structure. *Remote Sens. Environ.* **1990**, *34*, 107–119.
22. Wegmüller, U.; Werner, C.L. SAR interferometric signatures of forest. *IEEE Trans. Geosci. Remote Sens.* **1995**, *33*, 1153–1161.
23. Zebker, H.A.; Villasenor, J. Decorrelation in interferometric radar echoes. *IEEE Trans. Geosci. Remote Sens.* **1992**, *30*, 950–959.
24. Wegmüller, U.; Werner, C. Retrieval of vegetation parameters with SAR interferometry. *IEEE Trans. Geosci. Remote Sens.* **1997**, *35*, 18–24.
25. Santoro, M.; Wegmueller, U.; Askne, J.I.H. Signatures of ERS-envisat interferometric SAR coherence and phase of short vegetation: An analysis in the case of maize fields. *IEEE Trans. Geosci. Remote Sens.* **2010**, *48*, 1702–1713.
26. Zalite, K.; Voormansik, K.; Praks, J.; Antropov, O.; Noorma, M. Towards detecting mowing of agricultural grasslands from multi-temporal COSMO-SkyMed data. In Proceedings of the 2014 IEEE International Geoscience and Remote Sensing Symposium (IGARSS), Quebec, QC, Canada, 13–18 July 2014, pp. 5076–5079.
27. Zalite, K.; Antropov, O.; Praks, J.; Voormansik, K.; Noorma, M. Monitoring of agricultural grasslands with time series of X-band repeat-pass interferometric SAR. *IEEE J. Sel. Top. Appl. Earth Obs. Remote Sens.* **2015**, *9*, 3687–3697.
28. Askne, J.I.H.; Dammert, P.B.G.; Ulander, L.M.H.; Smith, G. C-band repeat-pass interferometric SAR observations of the forest. *IEEE Trans. Geosci. Remote Sens.* **1997**, *35*, 25–35.
29. Askne, J.; Santoro, M.; Smith, G.; Fransson, J.E.S. Multitemporal repeat-pass SAR interferometry of boreal forests. *IEEE Trans. Geosci. Remote Sens.* **2003**, *41*, 1540–1550.
30. Proisy, C.; Sarti, F.; Mougin, E.; Lopes, A.; Dufrene, E.; LeDantec, V.; Ruiz, C.; Borderies, P.; Chenerie, I. Temporal variations of interferometric coherence over a deciduous forest. In Proceedings of the SAR Workshop: CEOS Committee on Earth Observation Satellites, Working Group on Calibration and Validation, Toulouse, France, 26–29 October 1999.
31. Santoro, M.; Askne, J.; Smith, G.; Fransson, J.E.S. Stem volume retrieval in boreal forests from ERS-1/2 interferometry. *Remote Sens. Environ.* **2002**, *81*, 19–35.
32. Yague-Martinez, N.; Prats-Iraola, P.; Rodriguez Gonzalez, F.; Brcic, R.; Shau, R.; Geudtner, D.; Eineder, M.; Bamler, R. Interferometric processing of sentinel-1 TOPS data. *IEEE Trans. Geosci. Remote Sens.* **2016**, *54*, 2220–2234.
33. Level-1 Interferometric Wide Swath SLC Products. Available online: <https://earth.esa.int/web/sentinel/interferometric-wide-swath-slc> (accessed on 27 June 2016).
34. Hanssen, R.F. *Radar Interferometry: Data Interpretation and Error Analysis*; Springer Science & Business Media: Houten, The Netherlands, 2001.
35. Just, D.; Bamler, R. Phase statistics of interferograms with applications to synthetic aperture radar. *Appl. Opt.* **1994**, *33*, 4361–4368.
36. Touzi, R.; Lopes, A.; Bruniquel, J.; Vachon, P.W. Coherence estimation for SAR imagery. *IEEE Trans. Geosci. Remote Sens.* **1999**, *37*, 135–149.
37. Heistermann, M.; Jacobi, S.; Pfaff, T. Technical Note: An open source library for processing weather radar data (wradlib). *Hydrol. Earth Syst. Sci.* **2013**, *17*, 863–871.
38. Kirstetter, P.E.; Delrieu, G.; Boudevillain, B.; Obled, C. Toward an error model for radar quantitative precipitation estimation in the Cévennes–Vivarais region, France. *J. Hydrol.* **2010**, *394*, 28–41.
39. Hunter, J.D. Matplotlib: A 2D graphics environment. *Comput. Sci. Eng.* **2007**, *9*, 90–95.
40. Yang, H.; Zhao, C.; Yang, G.; Li, Z.; Chen, E.; Yuan, L.; Yang, X.; Xu, X. Agricultural crop harvest progress monitoring by fully polarimetric synthetic aperture radar imagery. *J. Appl. Remote Sens.* **2015**, *9*, 096076.
41. Adams, J.R.; Rowlandson, T.L.; McKeown, S.J.; Berg, A.A.; McNairn, H.; Sweeney, S.J. Evaluating the Cloude–Pottier and Freeman–Durden scattering decompositions for distinguishing between unharvested and post-harvest agricultural fields. *Can. J. Remote Sens.* **2013**, *39*, 318–327.

42. Ahmed, R.; Siqueira, P.; Hensley, S.; Chapman, B.; Bergen, K. A survey of temporal decorrelation from spaceborne L-Band repeat-pass InSAR. *Remote Sens. Environ.* **2011**, *115*, 2887–2896.
43. Hajj, M.E.; Baghdadi, N.; Belaud, G.; Zribi, M.; Cheviron, B.; Courault, D.; Hagolle, O.; Charron, F. Irrigated grassland monitoring using a time series of terraSAR-X and COSMO-skyMed X-Band SAR Data. *Remote Sens.* **2014**, *6*, 10002–10032.



© 2016 by the authors; licensee MDPI, Basel, Switzerland. This article is an open access article distributed under the terms and conditions of the Creative Commons Attribution (CC-BY) license (<http://creativecommons.org/licenses/by/4.0/>).